Formation of ZnO/Zn$_{0.5}$Cd$_{0.5}$Se Alloy Quantum Dots in the Presence of High Oleylamine Contents

Yi-An Chen [1,2], Kuo-Hsien Chou [1], Yi-Yang Kuo [1], Cheng-Ye Wu [1], Po-Wen Hsiao [1], Po-Wei Chen [1], Shuo-Huang Yuan [1] and Dong-Sing Wuu [1,2,3,*]

[1] Department of Materials Science and Engineering, National Chung Hsing University, 145 Xingda Road, Taichung 40227, Taiwan

[2] Innovation and Development Center of Sustainable Agriculture, National Chung Hsing University, Taichung 40227, Taiwan

[3] Research Center for Sustainable Energy and Nanotechnology, National Chung Hsing University, Taichung 40227, Taiwan

[*] Correspondence: dsw@nchu.edu.tw; Tel.: +886-4-22840500 (ext. 714); Fax: +886-4-22855046

Abstract: To the best of our knowledge, this report presents, for the first time, the schematic of the possible chemical reaction for a one-pot synthesis of Zn$_{0.5}$Cd$_{0.5}$Se alloy quantum dots (QDs) in the presence of low/high oleylamine (OLA) contents. For high OLA contents, high-resolution transmission electron microscopy (HRTEM) results showed that the average size of Zn$_{0.5}$Cd$_{0.5}$Se increases significantly from 4 to 9 nm with an increasing OLA content from 4 to 10 mL. First, [Zn(OAc)$_2$]–OLA complex can be formed by a reaction between Zn(OAc)$_2$ and OLA. Then, Fourier transform infrared (FTIR) spectroscopy and X-ray diffraction (XRD) data confirmed that ZnO is formed by thermal decomposition of the [Zn(OAc)$_2$]–OLA complex. The results indicated that ZnO grew on the Zn$_{0.5}$Cd$_{0.5}$Se surface, thus increasing the particle size. For low OLA contents, HRTEM images were used to estimate the average sizes of the Zn$_{0.5}$Cd$_{0.5}$Se alloy QDs, which were approximately 8, 6, and 4 nm with OLA loadings of 0, 2, and 4 mL, respectively. We found that Zn(OAc)$_2$ and OLA could form a [Zn(OAc)$_2$]–OLA complex, which inhibited the growth of the Zn$_{0.5}$Cd$_{0.5}$Se alloy QDs, due to the decreasing reaction between Zn(oleic acid)$_2$ and Se^{2-}, which led to a decrease in particle size.

Keywords: quantum dots; ZnO; one-pot method; Zn$_{0.5}$Cd$_{0.5}$Se; oleylamine

1. Introduction

The preparation and identification of quantum dots (QDs) have been widely studied, thus creating a new field of research. Different chemical methods have been reported for preparing QDs, such as microwave irradiation [1], solvothermal [2], and nonorganometallic precursor [3–5] methods, as well as the pyrolysis of single-molecular organometallic compounds [6,7], the organometallic precursor method [8], and the sonochemical method [9]. Preparing multicomponent alloy QDs involves more complicated steps than preparing single-component QDs. Thus, the fabrication of alloy QDs using the one-pot method has become a popular research topic since the late 2000s [10–15]. QDs have been used in a wide variety of applications such as light-emitting diodes, lasers [16,17], solar cells [18–20], photonic band-gap crystals [21], and biomedical labels [22–24]. QDs are quasi-zero-dimensional nanomaterials composed of typical inorganic semiconductors [25]. Because QDs have various emission wavelengths, they have attracted considerable attention in fields requiring special material, physical, and chemical properties [14,26]. The various emission wavelengths of multicomponent alloy QDs are the most widely investigated, given that many reaction parameters can be controlled. Although the

emission wavelength of QDs can change with nanoparticle size, it can also be controlled through the ratio and composition of the precursors [14].

More recently, various ligands, such as trioctylphosphine (TOP) ligands, oleic acid (OA) ligands, and oleylamine (OLA) ligands, have been extensively investigated in order to determine the impact of size and ligand chemistry on the optical properties and growth of QDs [27,28]. Most researchers have focused on changing the emission wavelength of QDs by controlling the reaction time, temperature, and ratio and composition of precursors [27–30]. The synthesis of ternary $Zn_xCd_{1-x}Se$ alloy QDs has become well-establishment using the one-pot method. Various shell/core QD systems have been synthesized and reported, i.e., $ZnS/Zn_xCd_{1-x}Se$, $CdZnS/Zn_xCd_{1-x}Se$, and $CdSe/Zn_xCd_{1-x}Se$, which are the most studied with simple synthetic control resulting in desired optical properties [30–34]. Previous studies have mostly used a two-step chemical reaction method to synthesize the core/shell ZnO/CdSe system and investigated emission wavelength, morphology, and growth evolution [35–38]. However, to the best of our knowledge, there are few reports on the core/shell $ZnO/Zn_xCd_{1-x}Se$ alloy QDs (not the $ZnO/Zn_xCd_{1-x}Se$ nanocables and hollow spheres) in the literature [19,39]. The effect of varying OLA contents on the growth evolution of $ZnO/Zn_xCd_{1-x}Se$ alloy QDs using a one-pot method has not yet been discussed. Thus, the growth evolution of $ZnO/Zn_xCd_{1-x}Se$ alloy QDs with various OLA contents is an important subject.

In the present study, we used a one-pot method to synthesize ternary $Zn_{0.5}Cd_{0.5}Se$ alloy QDs. We investigated the effect of the OLA ligands on the emission wavelength, morphology, and growth evolution of these QDs, which were characterized along with their structure using high-resolution transmission electron microscopy (HRTEM), photoluminescence (PL), Fourier transform infrared (FTIR) spectroscopy, ultraviolet-visible (UV-vis) spectroscopy, X-ray photoelectron spectroscopy (XPS), and X-ray diffraction (XRD).

2. Materials and Methods

2.1. Materials

Zinc acetate ($Zn(OAc)_2$, 99.99%), cadmium oxide (CdO, 99.99%), Se (99.99%), trioctylphosphine (TOP, 90%), 1-octadecene (ODE, 90%), OA (90%), OLA (80–90%), ethanol, and anhydrous toluene were purchased from Sigma-Aldrich (Uni-onward Trade Co., Ltd., New Taipei City, Taiwan) and used without any further purification.

2.2. Synthesis of $Zn_{0.5}Cd_{0.5}Se$ Alloy QDs

Three different $Zn_xCd_{1-x}Se$ alloy QDs were prepared using a one-pot method. The feed $Zn(OAc)_2$/CdO molar ratios were 0.5:0.5; the resulting products are hereinafter referred to as $Zn_{0.5}Cd_{0.5}Se$. To synthesize $Zn_{0.5}Cd_{0.5}Se$ alloy QDs, 0.5 mmol of $Zn(OAc)_2$, 0.5 mmol of CdO, and 5 mL of OA were placed in a four-neck flask along with different amounts of OLA (0, 2, 4, 6, or 10 mL) and ODE (10, 8, 6, 4, or 0 mL). Then, the mixture was heated to 150 °C under flowing high-purity Ar gas for 30 min. After 30 min, all the solids in the flask were completely dissolved, yielding a clear solution of $Zn(OA)_2$ and $Cd(OA)_2$. The solution was then heated to 300 °C while quickly injecting 4 mmol of Se in 4 mL of TOP into the four-neck flask. The reaction temperature was maintained at 280 °C for 30 min to grow the $Zn_{0.5}Cd_{0.5}Se$ alloy QDs. This solution was then rapidly added to ice toluene to terminate the reaction. The mixed solution was precipitated in excess ethanol and centrifuged at 5000 rpm for 10 min to separate the $Zn_{0.5}Cd_{0.5}Se$ alloy QDs and the supernatant liquid phase was decanted to remove the excess reagent. Subsequently, purified $Zn_{0.5}Cd_{0.5}Se$ alloy QDs in a nonpolar toluene solution were re-dispersed.

The alloy QDs are labeled $Zn_{0.5}Cd_{0.5}Se$-y, where y is the OLA content (mL) added during the synthesis process.

2.3. HRTEM

The morphology and size of all QDs were investigated using HRTEM (JEM-2100F, JEOL Ltd., Tokyo, Japan) with an accelerating voltage of 200 kV.

2.4. XRD

To determine the crystal structure of the QDs, XRD patterns were recorded using a Bruker D8 Advance diffractometer (Bruker AXS, Inc., Madison, WI, USA) over scanning ranges from $2\theta = 20°$ to $70°$ at a scanning rate of $2°$/min.

2.5. PL

The PL spectra were collected using a Hitachi F-2700 (Hitachi Ltd., Tokyo, Japan) fluorescence (excitation wavelength, $\lambda_{ex} = 365$ nm).

2.6. FTIR

The FTIR spectra were obtained on a Perkin-Elmer spectrometer (Waltham, MA, USA). One spectrum in the transmission mode from 400 to 4000 cm^{-1} was obtained after 20 scans at a 4 cm^{-1} resolution using the standard KBr disk method.

2.7. XPS

The chemical states and constituent compositions of the all samples were analyzed by XPS (ULVAC-PHI PHI 5000 Versa Probe, Kanagawa, Japan).

2.8. UV-vis Spectrophotometer

UV-vis spectra were performed on a Hitachi U-3010 (Hitachi Ltd., Tokyo, Japan) with a bandwidth 0.1 nm and a scanning speed at 200 nm/min.

3. Results and Discussion

3.1. Effect of Low OLA Content

According to the literature, both zinc-blende and wurtzite phases might form during the fabrication of ternary $Zn_{0.5}Cd_{0.5}Se$ alloy QDs [31–33]. We studied the effect of low OLA content on the preparation of $Zn_{0.5}Cd_{0.5}Se$ alloy QDs, where the initial OLA content was set to 0, 2, and 4 mL, and all other reaction parameters were fixed. All data were analyzed under the same parameters. Figure 1 shows the XRD patterns of $Zn_{0.5}Cd_{0.5}Se$ alloy QDs prepared with various OLA contents. The patterns of pure $Zn_{0.5}Cd_{0.5}Se$ alloy QDs clearly exhibited diffraction peaks at $2\theta = 25.32°$ (100), 26.63° (002), 28.29° (101), 37.24° (102), 44.78° (110), 48.33° (103), and 53.07° (112), indicating a wurtzite crystal structure [31,34]. Because the wurtzite phase is thermodynamically more stable than the zinc-blende phase [34], these ternary pure $Zn_{0.5}Cd_{0.5}Se$ alloy QDs predominantly developed a wurtzite structure. Thus, the $Zn_{0.5}Cd_{0.5}Se$ alloy QDs with various OLA contents all exhibited a wurtzite crystal structure [31,34]. The crystal structures of $Zn_{0.5}Cd_{0.5}Se$-2 and $Zn_{0.5}Cd_{0.5}Se$-4 alloy QDs are the same as that of pure $Zn_{0.5}Cd_{0.5}Se$ alloy QDs. These results suggest that adding OLA during synthesis does not change the crystal structure of $Zn_{0.5}Cd_{0.5}Se$ alloy QDs.

Figure 2 shows the HRTEM images and size distributions of various OLA contents on the preparation of $Zn_{0.5}Cd_{0.5}Se$ alloy QDs. In these images, all alloy QDs are clearly monodispersed and quasi-spherical. The average diameters of the $Zn_{0.5}Cd_{0.5}Se$ alloy QDs are estimated to be approximately 8, 6, and 4 nm for 0, 2, and 4 mL OLA loadings, respectively. Thus, the average diameters of the $Zn_{0.5}Cd_{0.5}Se$ alloy QDs decreases as the OLA content increases in the reaction solution up to 4 mL. This decrease might be due to OLA inhibiting the growth of $Zn_{0.5}Cd_{0.5}Se$ alloy QDs, thus decreasing the particle size (discussed in Section 3.2). In addition, the interplanar distances are estimated to be

0.37, 0.36, and 0.36 nm for pure $Zn_{0.5}Cd_{0.5}Se$, $Zn_{0.5}Cd_{0.5}Se$-2, and $Zn_{0.5}Cd_{0.5}Se$-4, respectively. This result suggests that adding OLA during synthesis does not change the crystal structure of $Zn_{0.5}Cd_{0.5}Se$ alloy QDs and consistent with the XRD results.
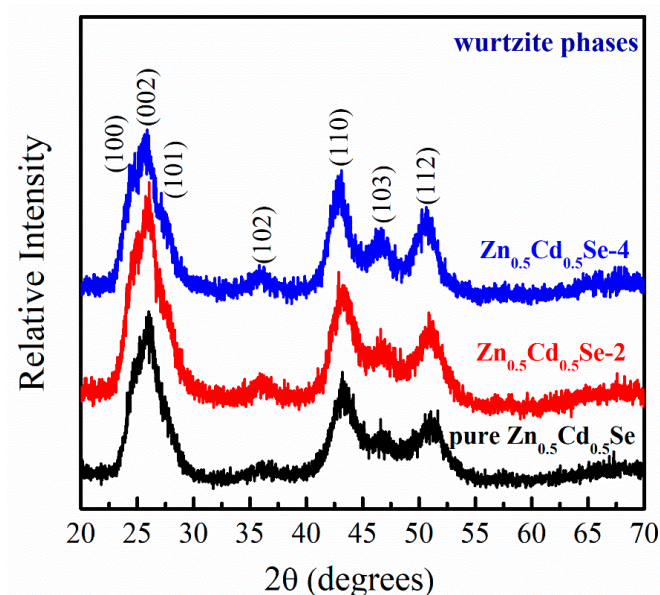
Figure 1. X-ray diffraction (XRD) patterns of $Zn_{0.5}Cd_{0.5}Se$ alloy quantum dots (QDs) with low oleylamine (OLA) content.
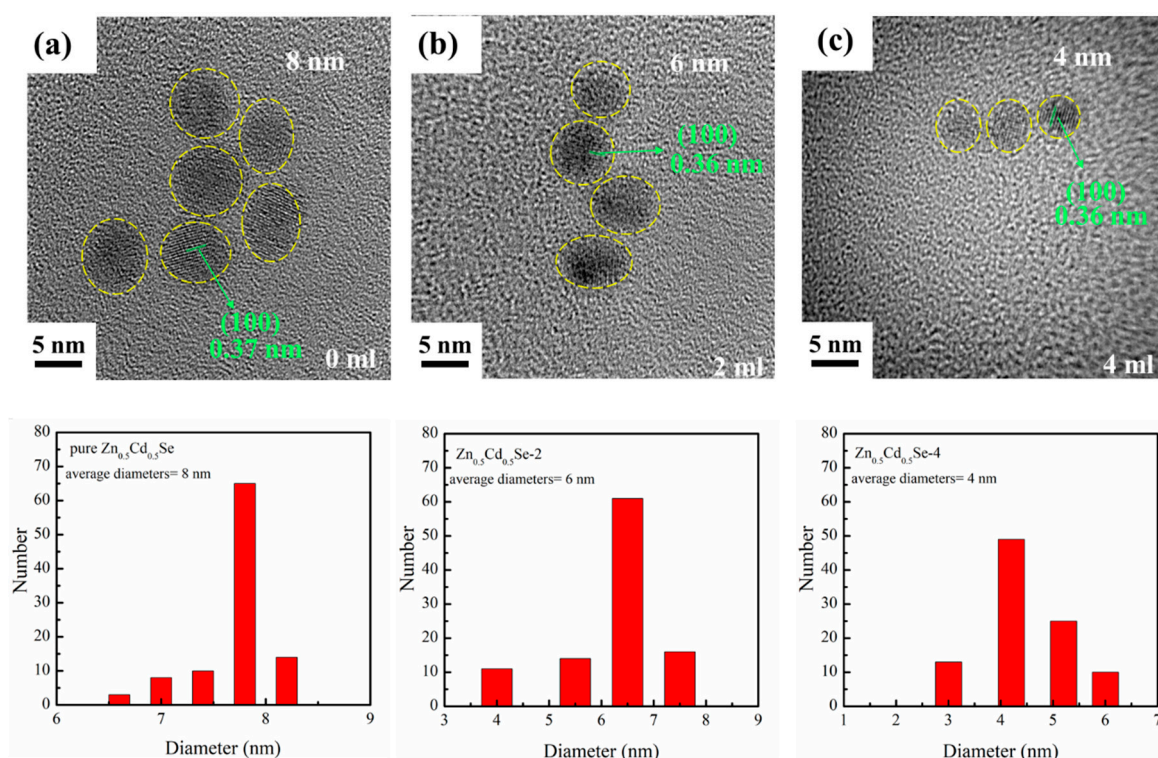
Figure 2. High-resolution transmission electron microscopy (HRTEM) images and size distributions showing the influence of low OLA content on (**a**) pure $Zn_{0.5}Cd_{0.5}Se$, (**b**) $Zn_{0.5}Cd_{0.5}Se$-2, and (**c**) $Zn_{0.5}Cd_{0.5}Se$-4 alloy QDs.

To understand the effect of adding OLA on the absorption and emission wavelength of $Zn_{0.5}Cd_{0.5}Se$ alloy QDs, UV-vis absorption and PL spectra were employed. The UV-vis absorption and PL spectra of $Zn_{0.5}Cd_{0.5}Se$ alloy QDs prepared with various OLA contents are shown in Figure 3. When the OLA content increased from 0 to 4 mL, the emission wavelength gradually blue-shifted from 671 to 651 nm, respectively. We observed that the first absorption feature blue-shifted from 649 to 635 nm. Thus, the absorption and emission wavelength of the $Zn_{0.5}Cd_{0.5}Se$ alloy QDs blue-shifted with decreasing particle size, which is the opposite trend as that of Cd_3P_2 QDs [29]. Specifically, Miao et al. reported that the emission peaks of Cd_3P_2 QDs red-shifted with increasing OLA content [29], which implied that adding OLA is helpful to the growth of Cd_3P_2 QDs [29].
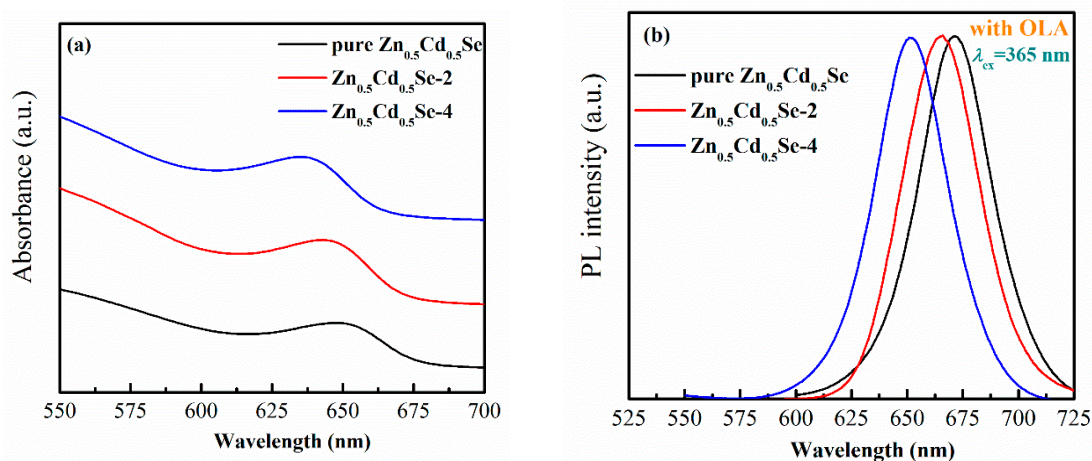
Figure 3. Influence of the low OLA content on the (**a**) UV-vis absorption spectra and (**b**) photoluminescence (PL) spectra of $Zn_{0.5}Cd_{0.5}Se$ alloy QDs.

3.2. Effect of High OLA Content

To investigate the crystal structure of pure $Zn_{0.5}Cd_{0.5}Se$ alloy QDs with high OLA contents, we recorded XRD patterns, which are depicted in Figure 4. The pure $Zn_{0.5}Cd_{0.5}Se$ alloy QDs exhibited a wurtzite crystal structure [31,34] and diffraction peaks at $2\theta = 25.32°, 26.63°, 28.29°, 37.24°, 44.78°, 48.33°,$ and $53.07°$ were assigned to the (100), (002), (101), (102), (110), (103), and (112) planes, respectively. The XRD patterns of $Zn_{0.5}Cd_{0.5}Se$-6 and $Zn_{0.5}Cd_{0.5}Se$-10 (Figure 4) containing six extra diffraction peaks were different from that of pure $Zn_{0.5}Cd_{0.5}Se$. Six diffraction peaks appeared at 2θ values of $31.80°, 34.41°, 36.21°, 56.53°, 62.74°,$ and $67.80°$, which correspond to the (100), (002), (101), (110), (103), and (112) planes of the wurtzite ZnO structure (JCPDS card no. 36-1451), respectively [40]. Since both $Zn_{0.5}Cd_{0.5}Se$ and ZnO have a wurtzite crystal structure, they provided good lattice matching. Thus, we conjectured that the wurtzite ZnO structure might preferentially grow on the $Zn_{0.5}Cd_{0.5}Se$ surface with high OLA contents.

To understand the XRD results, FTIR was used to explain the differences between $Zn_{0.5}Cd_{0.5}Se$ and $Zn_{0.5}Cd_{0.5}Se$-y. Figure 5 presents the FTIR spectra of $Zn_{0.5}Cd_{0.5}Se$ and $Zn_{0.5}Cd_{0.5}Se$-y. For all samples, the FTIR data revealed strong absorption peaks at 2986–3686 cm^{-1}, which were assigned to the carboxylic acid OH stretching mode of OA and N–H stretching vibration of OLA. The strong absorption peaks at 2853–3005 cm^{-1} were attributed to the =C–H and C–H stretching vibration of ligands (OA and/or OLA). The absorption peaks of the ligands (OA and/or OLA) are located in the wavenumber region from 630 to 1750 cm^{-1}. However, compared to the FTIR spectra of $Zn_{0.5}Cd_{0.5}Se$, $Zn_{0.5}Cd_{0.5}Se$-2 and $Zn_{0.5}Cd_{0.5}Se$-4, the FTIR spectra of $Zn_{0.5}Cd_{0.5}Se$-6 and $Zn_{0.5}Cd_{0.5}Se$-10 contained two extra absorption peaks at 530 and 435 cm^{-1}. The absorption peaks associated with Zn-O stretching band clearly appeared at 530 and 435 cm^{-1}, confirming the formation of ZnO [41]. These results demonstrate that this chemical reaction could produce ZnO when with high OLA contents.
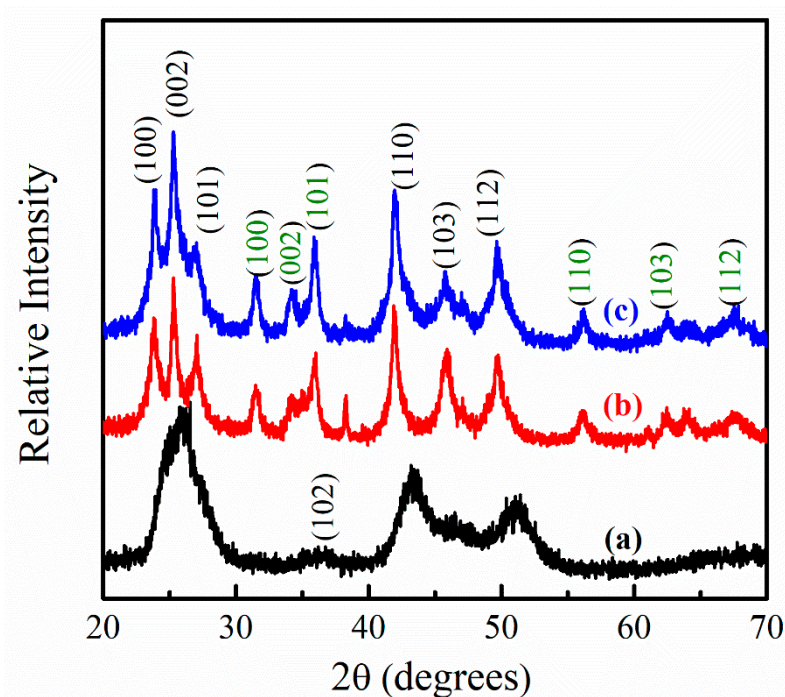
Figure 4. Effect of the high OLA content on the XRD patterns of (**a**) pure $Zn_{0.5}Cd_{0.5}Se$, (**b**) $Zn_{0.5}Cd_{0.5}Se$-6, and (**c**) $Zn_{0.5}Cd_{0.5}Se$-10 alloy QDs.
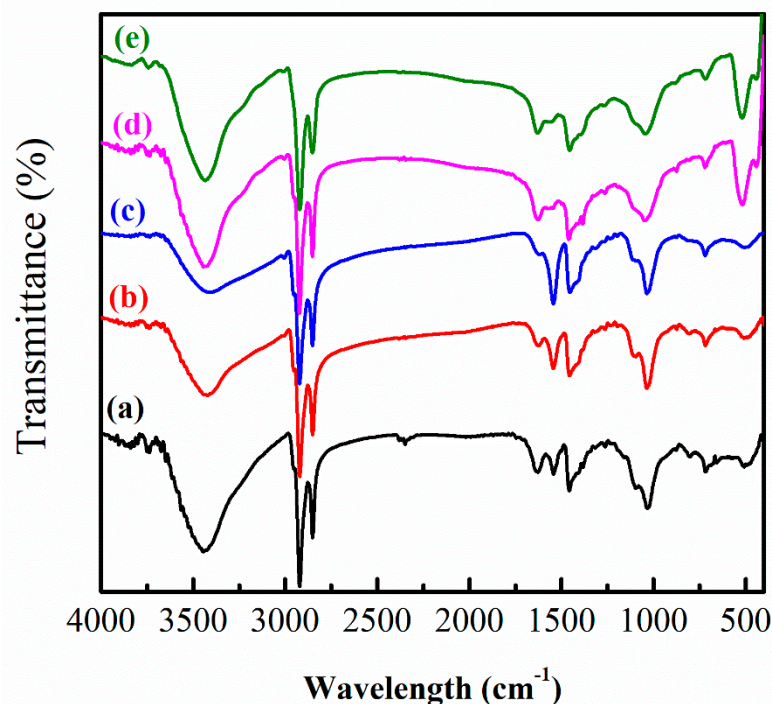
Figure 5. FTIR spectra showing the influence of the various OLA content on (**a**) pure $Zn_{0.5}Cd_{0.5}Se$, (**b**) $Zn_{0.5}Cd_{0.5}Se$-2, (**c**) $Zn_{0.5}Cd_{0.5}Se$-4, (**d**) $Zn_{0.5}Cd_{0.5}Se$-6, and (**e**) $Zn_{0.5}Cd_{0.5}Se$-10 alloy QDs.

To further explain the chemical states and constituent compositions, XPS spectra were analyzed. Figure 6 shows the XPS spectra of $Zn_{0.5}Cd_{0.5}Se$ and $Zn_{0.5}Cd_{0.5}Se$-y samples. In Figure 6a, two peaks (all samples) with binding energies of 404.5 and 411.3 eV can be attributed to Cd 3d [42]. The Se $3d_{5/2}$ and Se $3d_{3/2}$ peaks (all samples) with binding energies of 53.7 and 54.6 eV, respectively, are attributed to the Se^{2-} in CdSe and ZnSe, thus confirming the formation of CdSe and ZnSe [42,43], as presented in

Figure 6b. In Figure 6c, one peak with binding energy of 1021.2 eV can be observed for $Zn_{0.5}Cd_{0.5}Se$, $Zn_{0.5}Cd_{0.5}Se$-4, and $Zn_{0.5}Cd_{0.5}Se$-6 alloy QDs, which is attributed to Zn^{2+} existing in the form of ZnSe [44,45]. For the $Zn_{0.5}Cd_{0.5}Se$-6 and $Zn_{0.5}Cd_{0.5}Se$-10 alloy QDs, the two peaks with binding energies of 1021.1 and 1022.7 eV (Figure 6c) can be found, which are assigned to Zn^{2+} in the form of ZnO and ZnSe [44]. As shown in Figure 6d, the XPS spectra can be fit to two peaks with binding energies of 531.2 and 533.1 eV for $Zn_{0.5}Cd_{0.5}Se$, $Zn_{0.5}Cd_{0.5}Se$-4, and $Zn_{0.5}Cd_{0.5}Se$-6 alloy QDs. The binding energy peak at 531.2 eV is attributed to the C–O and C=O bands of oleic acid. The binding energy peak at 533.1 eV is correspondingly attributed to the O–C=O groups of oleic acid [46]. The results indicate that this chemical reaction could not produce ZnO with low OLA contents. For the $Zn_{0.5}Cd_{0.5}Se$-6 and $Zn_{0.5}Cd_{0.5}Se$-10 alloy QDs (Figure 6d), the O–C=O binding energy peak of oleic acid also appears at 533.1 eV. We also observed that the binding energy peak at 529.9eV is attributed to O^{2-} in ZnO, thus confirming the formation of ZnO [45]. Consequently, the addition of high OLA contents could form $ZnO/Zn_{0.5}Cd_{0.5}Se$ QDs in this chemical reaction process.
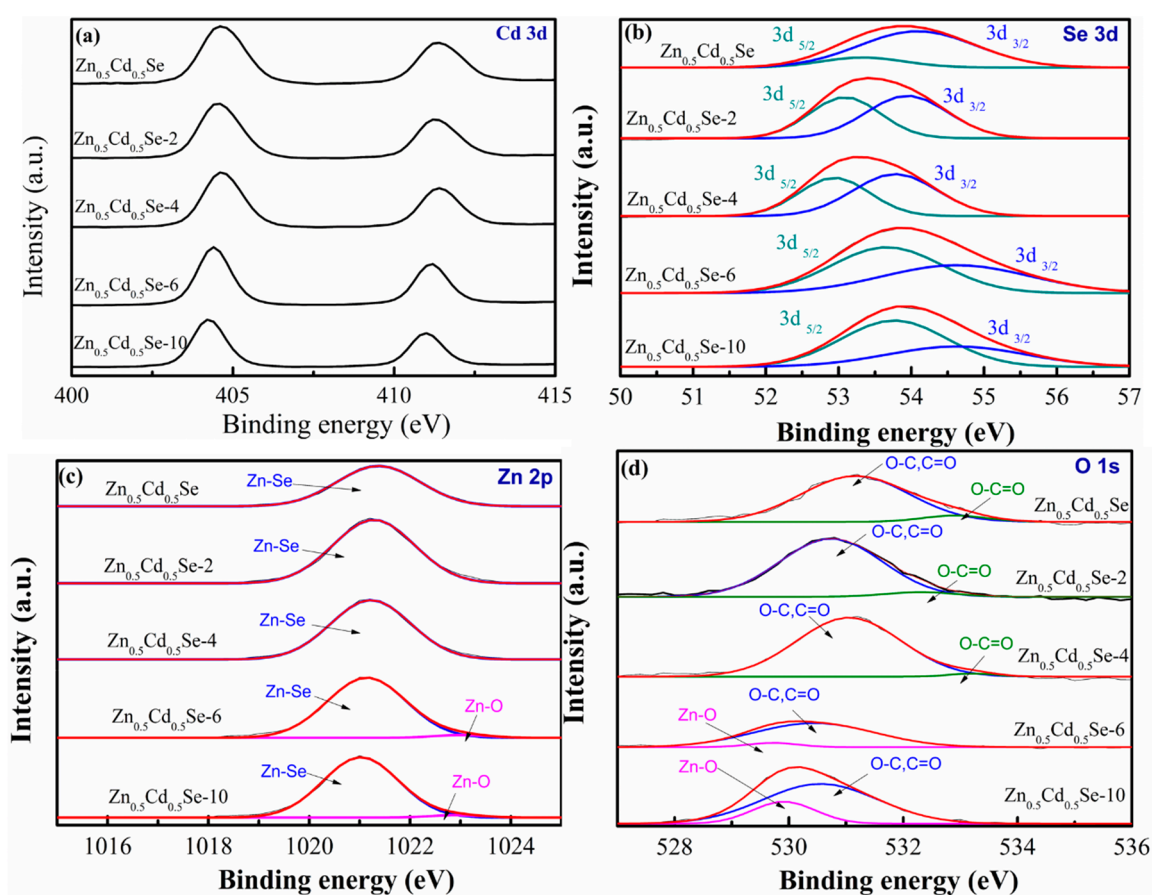
Figure 6. (**a**) Cd 3d, (**b**) Se 3d, (**c**) Zn 2p, and (**d**) O 1s X-ray photoelectron spectroscopy (XPS) spectra showing the influence of the various OLA content on $Zn_{0.5}Cd_{0.5}Se$ and $Zn_{0.5}Cd_{0.5}Se$-y.

As shown in Figure 7a,b, the HRTEM images and size distributions of $Zn_{0.5}Cd_{0.5}Se$-6 and $Zn_{0.5}Cd_{0.5}Se$-10 were captured. These figures demonstrate that the $Zn_{0.5}Cd_{0.5}Se$-6 and $Zn_{0.5}Cd_{0.5}Se$-10 alloy QDs were fully crystalline. Further, they exhibited well-resolved lattice fringes. We clearly observed that adding a high content of OLA during synthesis does not affect the interplanar distances of $Zn_{0.5}Cd_{0.5}Se$. In addition, the average diameters were estimated to be approximately 6 and 9 nm for $Zn_{0.5}Cd_{0.5}Se$-6 and $Zn_{0.5}Cd_{0.5}Se$-10, respectively. The average diameters of the $Zn_{0.5}Cd_{0.5}Se$ alloy QDs increased as the OLA content increased in the reaction solution from 4 (Figure 2c) to 10 mL. In these images, we found that a thin layer grew on the surface of $Zn_{0.5}Cd_{0.5}Se$ alloy QDs. This increase might be due to ZnO growing on the $Zn_{0.5}Cd_{0.5}Se$ surface, thus increasing the particle size.
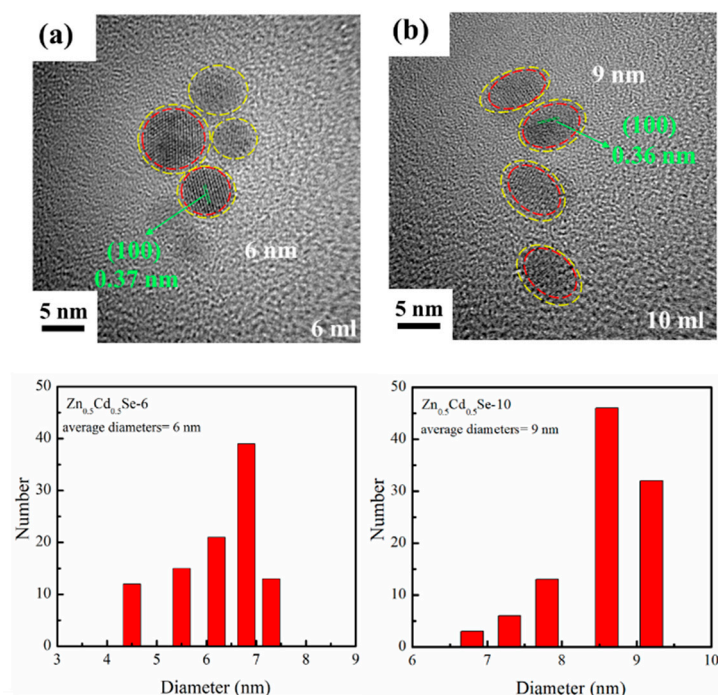
Figure 7. HRTEM images and size distributions showing the influence of the high OLA contents on the (**a**) $Zn_{0.5}Cd_{0.5}Se$-6 and (**b**) $Zn_{0.5}Cd_{0.5}Se$-10 alloy QDs.

Figure 8 shows the UV-vis absorption and PL spectra of $Zn_{0.5}Cd_{0.5}Se$ alloy QDs prepared with high OLA contents. After overcoating the $Cd_{0.5}Zn_{0.5}Se$ with the ZnO shell, the absorption wavelengths of $Zn_{0.5}Cd_{0.5}Se$-6 and $Zn_{0.5}Cd_{0.5}Se$-10 QDs exhibited a redshift (from 635 to 654 nm) compared to $Cd_{0.5}Zn_{0.5}Se$-4 QD, as shown in Figure 8a. Figure 8b shows that the emission peak red-shifted from 651 to 676 nm. The results indicate that ZnO can form in this reaction that grows on the $Zn_{0.5}Cd_{0.5}Se$ surface due to the increasing reaction between $[Zn(OAc)_2]$–OLA complex, TOP, and oxygen ion [47–49], thus increasing the particle size and red-shifting the absorption and emission wavelengths. In addition, the photoluminescence quantum yield (PL QY) of all samples with different OLA contents was monitored, calculated by comparison with standard organic dye. The PL QY was estimated to be approximately 21.5%, 14.9%, 13.7%, 23.7%, and 26.5% for pure $Zn_{0.5}Cd_{0.5}Se$, $Zn_{0.5}Cd_{0.5}Se$-2, $Zn_{0.5}Cd_{0.5}Se$-4, $Zn_{0.5}Cd_{0.5}Se$-6, and $Zn_{0.5}Cd_{0.5}Se$-10, respectively. The PL QY first decreased and then increased with increasing OLA content. This indicates that after $Zn_{0.5}Cd_{0.5}Se$ cores being coated with ZnO, the PL QY of $Zn_{0.5}Cd_{0.5}Se$-6 and $Zn_{0.5}Cd_{0.5}Se$-10 obviously enhanced. This phenomenon can be explained by ZnO having a low lattice mismatch with $Zn_{0.5}Cd_{0.5}Se$, and ZnO can provide strong confinement for the $Zn_{0.5}Cd_{0.5}Se$ QD cores as well as remove their surface defects [33,35–38].

To understand all chemical reaction mechanisms, we propose a schematic of the possible reaction mechanism underlying the chemical synthesis for the one-pot method for $Zn_{0.5}Cd_{0.5}Se$ alloy QDs with low/high OLA contents, as shown in Figure 9. Figure 9a illustrates that the precursors (CdO and $Zn(OAc)_2$) in the OA and ODE solution formed $Zn(OA)_2$ and $Cd(OA)_2$ when the reaction temperature reached 150 °C. When the reaction temperature reached 300 °C, the Se-TOP solution was quickly injected into the reaction solution. At this time, $Zn_{0.5}Cd_{0.5}Se$ alloy began to form. Subsequently, the reaction temperature was maintained at 280 °C to grow the $Zn_{0.5}Cd_{0.5}Se$ alloy QDs. This reaction process occurred without the presence of OLA. Figure 9c illustrates the probable chemical synthesis mechanism underlying the growth of $Zn_{0.5}Cd_{0.5}Se$ alloy QDs in the presence of high OLA contents. It is known that ZnO nanoparticles can be formed through thermal decomposition of $Zn(OAc)_2$ or $Zn(acac)_2$ [47–49]. The literature indicates that before the formation of ZnO nanoparticles, $Zn(OAc)_2$ and OLA can form the $[Zn(OAc)_2]$–OLA complex as precursors. In this study, when the reaction

temperature reached 150 °C, the precursors (CdO and Zn(OAc)$_2$) in the OA, OLA, and ODE solution formed Zn(OA)$_2$, Cd(OA)$_2$, and the [Zn(OAc)$_2$]–OLA complex, respectively. Then, cadmium oxide dissociated into cadmium ions and oxygen ions. The [Zn(OAc)$_2$]–OLA complex, TOP, and oxygen ion at 280 °C were used to form ZnO via the thermal decomposition with high OLA contents. FTIR, XPS, and XRD data also confirmed that the addition of high OLA contents could form the ZnO/Zn$_{0.5}$Cd$_{0.5}$Se QDs in this chemical reaction process. Thus, the HRTEM results demonstrate that this increase might be due to the ZnO growing on the Zn$_{0.5}$Cd$_{0.5}$Se surface, thus increasing the particle size.
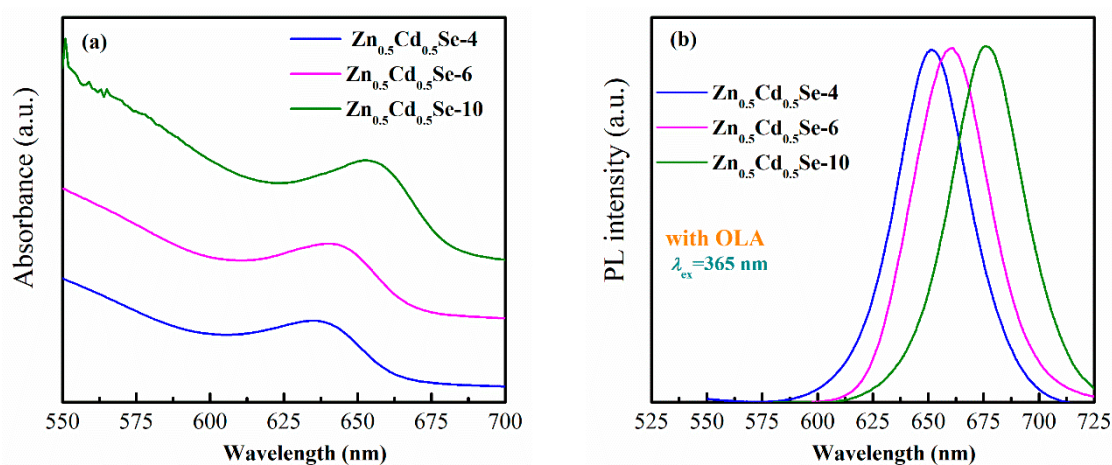
Figure 8. Influence of the high OLA content on the (**a**) UV-vis absorption spectra and (**b**) PL spectra of Zn$_{0.5}$Cd$_{0.5}$Se alloy QDs.
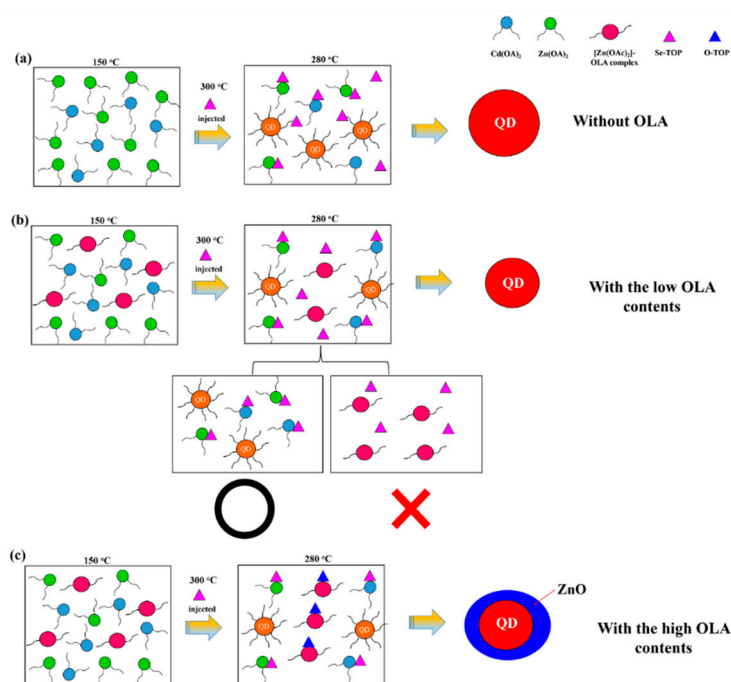
Figure 9. Schematic diagrams of the possible chemical reaction mechanisms underlying the one-pot chemical synthesis of Zn$_{0.5}$Cd$_{0.5}$Se alloy QDs (**a**) without OLA, (**b**) with low OLA contents, and (**c**) with high OLA contents.

According to the literatures [47–49] and above results, we also confirmed that the chemical reaction could produce [Zn(OAc)$_2$]–OLA complexes with the addition of low OLA contents (Section 3.1). Because the OLA contents were too low, this chemical reaction could not produce ZnO/Zn$_{0.5}$Cd$_{0.5}$Se QDs (Figures 1 and 5). When the reaction temperature was maintained at 280 °C, only some Zn(OA)$_2$

chemically reacted. This phenomenon indicates that the [Zn(OAc)$_2$]–OLA complex inhibits the growth of Zn$_{0.5}$Cd$_{0.5}$Se alloy QDs because of the reduction in the reaction between Zn(OA)$_2$ and Se^{2-}, which leads to a decrease in the particle size, as shown in Figure 9b. Therefore, the Zn$_{0.5}$Cd$_{0.5}$Se alloy QD produces a blue shift of its emission wavelength with increasing the OLA amount (from 0 to 4 mL).

4. Conclusions

To the best of our knowledge, a schematic diagram of the possible mechanism for the one-pot synthesis of Zn$_{0.5}$Cd$_{0.5}$Se alloy QDs in the presence of low/high OLA contents is reported for the first time. Under the condition of high OLA contents, the average size of Zn$_{0.5}$Cd$_{0.5}$Se QD examined by HRTEM increases significantly from 4 to 9 nm when the OLA content increases from 4 to 10 mL. In the beginning, the [Zn(OAc)$_2$]–OLA complex can be formed via a reaction between Zn(OAc)$_2$ and OLA. Then, the thermal decomposition of [Zn(OAc)$_2$]–OLA complexes occurs and forms the ZnO as confirmed by the FTIR, XRD, and XPS measurements. The results indicate that the ZnO can grow on the Zn$_{0.5}$Cd$_{0.5}$Se surface, thus increasing the particle size. For the QD synthesized under low OLA loadings of 0, 2, and 4 mL, the average sizes of the Zn$_{0.5}$Cd$_{0.5}$Se alloy QDs are approximately 8, 6, and 4 nm as estimated by HRTEM, respectively. It could be due to the reduction in the reaction between Zn(OA)$_2$ and Se^{2-}, which led to a decrease in the particle size. Therefore, the emission wavelengths of the Zn$_{0.5}$Cd$_{0.5}$Se alloy QDs are blue-shifted with the increase of the OLA amount from 0 to 4 mL.

References

1.　Zhu, J.J.; Palchik, O.; Chen, S.; Gedanken, A. Microwave assisted preparation of CdSe, PbSe, and Cu$_{2-x}$Se nanoparticles. *J. Phys. Chem. B* **2000**, *31*, 7344–7347. [CrossRef]

2.　Xun, W.; Jing, Z.; Qing, P.; Yadong, L. A general strategy for nanocrystal synthesis. *Nature* **2005**, *437*, 121–124.

3.　Peng, Z.A.; Peng, X.G. Formation of high-quality CdTe, CdSe, and CdS nanocrystals using CdO as precursor. *J. Am. Chem. Soc.* **2001**, *123*, 183–184. [CrossRef] [PubMed]

4.　Lianhua, Q.; Adam, P.Z.; Xiaogang, P. Alternative routes toward high quality CdSe nanocrystals. *Nano Lett.* **2001**, *1*, 333–337.

5.　Craig, R.B.; Paul, M. Nucleation and growth kinetics of CdSe nanocrystals in octadecene. *Nano Lett.* **2004**, *4*, 2303–2307.

6.　Green, M.; O'Brien, P. Recent advances in the preparation of semiconductors as isolated nanometric particles: New routes to quantum dots. *Chem. Commun.* **1999**, *22*, 2235–2241. [CrossRef]

7.　Cumberland, S.L.; Hanif, K.M.; Javier, A.; Khitrov, G.A.; Strouse, G.F.; Woesser, S.M.; Yun, C.S. Inorganic clusters as single-source precursors for preparation of CdSe, ZnSe, and CdSe/ZnS nanomaterials. *Chem. Mater.* **2002**, *14*, 1576–1584. [CrossRef]

8.　Qu, L.H.; Peng, X.G. Control of photoluminescence properties of CdSe nanocrystals in growth. *J. Am. Chem. Soc.* **2002**, *124*, 2049–2055. [CrossRef]

9.　Ge, J.P.; Li, Y.D.; Yang, G.Q. Mechanism of aqueous ultrasonic reaction: Controlled synthesis, luminescence properties of amorphous cluster and nanocrystalline CdSe. *Chem. Commun.* **2002**, *17*, 1826–1827. [CrossRef]

10.　Chung, S.R.; Siao, C.B.; Wang, K.W. Full color display fabricated by CdSe bi-color quantum dots-based white light-emitting diodes. *Opt. Mater. Express* **2018**, *8*, 2677–2686. [CrossRef]

11.　Jeong, D.W.; Parka, J.Y.; Seoa, H.W.; Myung, N.V.; Seong, T.Y.; Kim, B.S. One-pot synthesis of gradient interface quaternary ZnCdSSe quantum dots. *Appl. Surf. Sci.* **2017**, *415*, 19–23. [CrossRef]

12. Jiaa, Y.; Wanga, H.; Xianga, L.; Liu, X.; Wei, W.; Ma, N.; Sun, D. Tunable emission properties of core-shell ZnCuInS-ZnS quantum dots with enhanced fluorescence intensity. *J. Mater. Sci. Technol.* **2018**, *4*, 942–948. [CrossRef]

13. Cho, J.; Jung, Y.K.; Lee, J.K.; Jung, H.S. Highly efficient blue-emitting CdSe-derived core/shell gradient alloy quantum dots with improved photoluminescent quantum yield and enhanced photostability. *Langmuir* **2016**, *33*, 3711–3719. [CrossRef] [PubMed]

14. Leea, H.; Yang, H.; Holloway, P.H. Single-step growth of colloidal ternary ZnCdSe nanocrystals. *J. Lumin.* **2007**, *126*, 314–318. [CrossRef]

15. Ouyang, J.; Vincent, M.; Kingston, D.; Descours, P.; Boivineau, T.; Zaman, M.B.; Wu, X.; Yu, K. Noninjection, one-pot synthesis of photoluminescent colloidal homogeneously alloyed CdSeS quantum dots. *J. Phys. Chem. C* **2009**, *113*, 5193–5200. [CrossRef]

16. Lee, J.S.; Kang, B.H.; Kim, S.H.; Lee, J.W.; Lee, S.W.; Kim, S.W.; Gopalan, S.A.; Kwon, J.B.; Bae, J.H.; Kim, E.S.; et al. All-solution-processed high-brightness hybrid white quantum-dot light-emitting devices utilizing polymer modified quantum dots. *Org. Electron.* **2017**, *42*, 393–398. [CrossRef]

17. Coe, S.; Woo, W.K.; Bawendi, M.; Bulović, V. Electroluminescence from single monolayers of nanocrystals in molecular organic devices. *Nature* **2002**, *420*, 800–803. [CrossRef] [PubMed]

18. Yu, L.; Li, Z. Synthesis of $Zn_xCd_{1-x}Se@ZnO$ hollow spheres in different sizes for quantum dots sensitized solar cells application. *Nanomaterials* **2019**, *9*, 132. [CrossRef] [PubMed]

19. Huynh, W.U.; Dittmer, J.J.; Alivisatos, A.P. Hybrid nanorod polymer solar cells. *Science* **2002**, *295*, 2425–2427. [CrossRef] [PubMed]

20. Gur, I.; Fromer, N.A.; Geier, M.L.; Alivisatos, A.P. Air-stable allinorganic nanocrystal solar cells processed from solution. *Science* **2005**, *310*, 462–465. [CrossRef] [PubMed]

21. Vlasov, Y.A.; Yao, N.; Norris, D.J. Synthesis of photonic crystals for optical wavelengths from semiconductor quantum dots. *Adv. Mater.* **1999**, *11*, 165–169. [CrossRef]

22. Bruchez, M.; Moronne, M.; Gin, P.; Weiss, S.; Alivisatos, A.P. Semiconductor nanocrystals as fluorescent biological labels. *Science* **1998**, *281*, 2013–2016. [CrossRef] [PubMed]

23. Talapin, D.V.; Lee, J.S.; Kovalenko, M.V.; Shevchenko, E.V. Prospects of colloidal nanocrystals for electronic and optoelectronic applications. *Chem. Rev.* **2010**, *110*, 389–458. [CrossRef] [PubMed]

24. Freeman, R.; Willner, I. Optical molecular sensing with semiconductor quantum dots (QDs). *Chem. Soc. Rev.* **2012**, *41*, 4067–4085. [CrossRef] [PubMed]

25. Zhang, L.J.; Xia, L.; Xie, H.Y.; Zhang, Z.L.; Pang, D.W. Quantum dot based biotracking and biodetection. *Anal. Chem.* **2019**, *91*, 532–547. [CrossRef] [PubMed]

26. Zhong, X.; Han, M.; Dong, Z.; White, T.J.; Knoll, W. Composition-tunable $Zn_xCd_{1-x}Se$ nanocrystals with high luminescence and stability. *J. Am. Chem. Soc.* **2003**, *125*, 8589–8594. [CrossRef]

27. Deng, Z.; Lie, F.L.; Shen, S.; Ghosh, I.; Mansuripur, M.; Muscat, A.J. Water-based route to ligand-selective synthesis of ZnSe and Cd-doped ZnSe quantum dots with tunable ultraviolet A to blue photoluminescence. *Langmuir* **2009**, *25*, 434–442. [CrossRef]

28. Cao, J.; Xue, B.; Li, H.; Deng, D.; Gu, Y. Facile synthesis of high-quality water-soluble N-acetyl-L-cysteine-capped $Zn_{1-x}Cd_xSe/ZnS$ core/shell quantum dots emitting in the violet–green spectral range. *J. Colloid Interface Sci.* **2010**, *348*, 369–376. [CrossRef]

29. Miao, S.; Hickey, S.G.; Rellinghaus, B.; Waurisch, C.; Eychmüller, A. Synthesis and characterization of cadmium phosphide quantum dots emitting in the visible red to near-infrared. *J. Am. Chem. Soc.* **2010**, *132*, 5613–5615. [CrossRef]

30. Yang, P.; Wang, S.; Ando, M.; Murase, N. CdSe/$Cd_{1-x}Zn_xS$ core/shell quantum dots with tunable emission: Growth and morphology evolution. *J. Mater. Sci.* **2013**, *48*, 651–658. [CrossRef]

31. Bailey, R.E.; Nie, S.M. Alloyed semiconductor quantum dots: Tuning the optical properties without changing the particle size. *J. Am. Chem. Soc.* **2003**, *125*, 7100–7106. [CrossRef] [PubMed]

32. Zheng, Y.G.; Yang, Z.C.; Ying, J.Y. Aqueous synthesis of glutathione-capped ZnSe and $Zn_{1-x}Cd_xSe$ alloyed quantum dots. *Adv. Mater.* **2007**, *19*, 1475–1479. [CrossRef]

33. Huang, C.H.; Yang, C.H.; Shieh, Y.T.; Wang, T.L. Synthesis and properties of alloyed $Cd_xZn_{1-x}Se$ core and manganese doped $Cd_xZn_{1-x}Se/ZnS$ core/shell nanocrystals. *J. Alloy. Compd.* **2018**, *748*, 265–272. [CrossRef]

34. Wei, H.; Su, Y.; Han, Z.; Li, T.; Ren, X.; Yang, Z.; Wei, L.; Cong, F.; Zhang, Y. $Zn_xCd_{1-x}Se$ nanomultipods with tunable band gaps: Synthesis and first-principles calculations. *Nanotechnology* **2013**, *24*, 235706. [CrossRef] [PubMed]

35. Nguyen, T.L.; Michael, M.; Mulvaney, P. Synthesis of Highly Crystalline CdSe@ZnO Nanocrystals via Monolayer-by-Monolayer Epitaxial Shell Deposition. *Chem. Mater.* **2014**, *26*, 4274–4279. [CrossRef]

36. An, L.; Chen, X.; Han, X.; Yi, J.; Liu, C.; An, W.; Qu, Y.; Chi, J.; Wei, H.; Wen, Y.; et al. CdSe/ZnO core/shell semiconductor nanocrystals: Synthesis and Characterization. *Appl. Mech. Mater.* **2013**, *268*, 207–210. [CrossRef]

37. Lu, Q.; Yubai Bai, G.S. Synthesis and characterization of CdSe/ZnO core/shell nanocrystals. *Int. J. Nanosci.* **2006**, *5*, 299–306. [CrossRef]

38. Aldeek, F.; Mustin, C.; Balan, L.; Medjahdi, G.; Roques-Carmes, T.; Arnoux, P.; Schneider, R. Enhanced photostability from CdSe(S)/ZnO core/shell quantum dots and their use in biolabeling. *Eur. J. Inorg. Chem.* **2011**, *2011*, 794–801. [CrossRef]

39. Zeng, Y.; Yang, T.; Li, C.; Xie, A.; Li, S.; Zhang, M.; Shen, Y. $Zn_xCd_{1-x}Se$ nanoparticles decorated ordered mesoporous ZnO inverse opal with binder-free heterojunction interfaces for highly efficient photoelectrochemical water splitting. *Appl. Catal. B Environ.* **2019**, *245*, 469–476. [CrossRef]

40. Fageria, P.; Gangopadhyay, S.; Pande, S. Synthesis of ZnO/Au and ZnO/Ag nanoparticles and their photocatalytic application using UV and visible light. *RSC Adv.* **2014**, *4*, 24962–24972. [CrossRef]

41. Khalaf, T.; Buazar, F.; Ghanemi, K. Phycosynthesis and enhanced photocatalytic activity of zinc oxide nanoparticles toward organosulfur pollutants. *Sci. Rep.* **2019**, *9*, 6866. [CrossRef] [PubMed]

42. Gakhar, R.; Merwin, A.; Summers, K.; Pilli, S.K.; Chidambaram, D. Application of $Zn_xCd_{1-x}Se$-sensitized TiO_2 nanotube arrays as photoanodes for solar cells. *J. Mater. Chem. A* **2014**, *2*, 10116–10125. [CrossRef]

43. Gualdrón-Reyes, A.F.; Meléndez, A.M.; Tirado, J.; Escobar, M.A.M.; Jaramillo, F.; Niño-Gómez, M.E. Hidden energy levels? Carrier transport ability of $CdS/CdS_{1-x}Se_x$ quantum dot solar cells impacted by Cd–Cd level formation. *Nanoscale* **2019**, *11*, 762–774. [CrossRef] [PubMed]

44. Cai, C.; Xu, Y.F.; Chen, H.Y.; Wang, X.D.; Kuang, D.B. Porous ZnO@ZnSe nanosheet array for photoelectrochemical reduction of CO_2. *Electrochim. Acta* **2018**, *274*, 298–305. [CrossRef]

45. Mittal, V.; Sessions, N.P.; Wilkinson, J.S.; Murugan, G.S. Optical quality ZnSe films and low loss waveguides on Si substrates for mid-infrared applications. *Opt. Mater. Express* **2017**, *3*, 712–725. [CrossRef]

46. Wilson, D.; Langell, M.A. XPS analysis of oleylamine/oleic acid capped Fe_3O_4 nanoparticles as a function of temperature. *Appl. Surf. Sci.* **2014**, *303*, 6–13. [CrossRef]

47. Masoud, S.N.; Davar, F.; Mazaheri, M. Preparation of ZnO nanoparticles from [bis(acetylacetonato)zinc(II)]–oleylamine complex by thermal decomposition. *Mater. Lett.* **2008**, *62*, 1890–1892.

48. Musić, S.; Šarić, A.; Popović, S. Formation of nanosize ZnO particles by thermal decomposition of zinc acetylacetonate monohydrate. *Ceram. Int.* **2010**, *36*, 1117–1123. [CrossRef]

49. Wood, A.; Giersig, M.; Hilgendorff, M.; Vilas-Campos, A.; Liz-Marzán, L.M.; Mulvaney, P. Size effects in ZnO: The cluster to quantum dot transition. *Aust. J. Chem.* **2003**, *56*, 1051–1057. [CrossRef]